Revisiting the Enhanced Chemical Reactivity in Water Microdroplets: The Case of a Diels-Alder Reaction

Ke Gong,[#,1] Abhijit Nandy,[#,2] Zhexuan Song,[1] Quan-Song Li,[1] Ali Hassanali,[3] Giuseppe Cassone,[*,4] Shibdas Banerjee,[*,2] Jing Xie[*,1]

[1]Key Laboratory of Cluster Science of Ministry of Education, Beijing Key Laboratory of Photoelectronic/Electrophotonic Conversion Materials, School of Chemistry and Chemical Engineering, Beijing Institute of Technology, Beijing 100081, China

[2]Department of Chemistry, Indian Institute of Science Education and Research Tirupati, Tirupati 517507, India

[3]International Centre for Theoretical Physics (ICTP), 34151 Trieste, Italy

[4] Institute for Physical-Chemical Processes, Italian National Research Council (CNR-IPCF), 98158 Messina, Italy

[*]Emails: giuseppe.cassone@ipcf.cnr.it; shibdas@iisertirupati.ac.in; jingxie@bit.edu.cn

ABSTRACT: Often, chemical reactions are markedly accelerated in microdroplets compared to the corresponding bulk-phase. While identifying the precise causative factors remains challenging, the interfacial electric field (IEF) and partial solvation are the two widely proposed factors, accounting for the acceleration or turning on many reactions in microdroplets. In sharp contrast, this combined computational and experimental study demonstrates that these two critical factors have negligible effect on promoting a model Diels-Alder (DA) reaction between cyclopentadiene and acrylonitrile in water microdroplets. Instead, the acceleration of the DA reaction appears to be driven by the effect of confinement and the concentration increase caused by evaporation. Quantum chemical calculations and *ab initio* molecular dynamics simulations coupled with enhanced sampling techniques predict that the air-water interface exhibits a higher free-energy barrier of this reaction than the bulk, while external electric fields marginally reduce the barrier. Remarkably, the catalytic capability of the IEF at the water microdroplet surface is largely hampered by its fluctuating character. Mass spectrometric assessment of the microdroplet reaction corroborate these findings, suggesting that the DA reaction is not facilitated by the IEF as increasing the spray potential suppresses the DA products by promoting substrate oxidation. While the DA reaction exhibits a surface preference in water microdroplets, the same reaction tends to occur mainly within the core of the acetonitrile microdroplet, suggesting the partial solvation is not necessarily a critical factor for accelerating this reaction in microdroplets. Moreover, experiments indicate that the rapid evaporation of microdroplets and the subsequent reagent enrichment within the accessible confined volume of microdroplets caused the observed acceleration of the DA reaction in water microdroplets.

INTRODUCTION

Converting bulk water into micron-sized droplets renders it to behave unusually, often facilitating the chemical transformation of species dissolved in it. The recent surge in such water microdroplet chemistry has been enriched by various studies, which include observations of accelerated reaction rates,[1-5] the promotion of unusual chemical reactions,[6-28] and the stabilization of highly reactive intermediates at the air-water interface.[29-31] The cause of such multifaceted chemistry, preferably at the air-water interface of microdroplets, is often attributed to a multitude of variables that the reactant species experiences at different extents depending upon the nature of the reactant. Some of the important variables driving the water microdroplet chemistry have been identified to be: i) high intrinsic electric fields (up to 10^9 V/m) at the droplet surface,[5, 22, 32-36] ii) orientation of reactant(s) at the droplet surface,[15] iii) partial solvation of reactant(s) at the air-water interface,[37-38] iv) droplet surface polarity or pH (acidity/basicity),[1, 39-44] v) confinement of reactants/reagents in small volumes,[4, 41, 45-46] vi) evaporation of droplet and thereby sizes and associated lifetimes.[4, 47-56]

Besides the preceding factors, impurities like ozone or other reactive oxygen species at the microdroplet interface have been suggested to influence the interfacial chemistry in microdroplets.[57-60] The origin of these impurities and reactive oxygen species, including H_2O_2, remains a topic of intense debate.[57, 60-68] Studies by Mishra and co-workers found no role of interfacial electric fields (IEF) in the formation of H_2O_2.[57, 63] Instead, they suggested the origins of H_2O_2 in water microdroplets is closely linked to the use of ultrasonic humidifiers, ambient ozone[57] or dissolved oxygen.[64] Zare and co-workers later affirmed that H_2O_2 can be formed in microdroplets in the absence of ozone, however, the quantity of H_2O_2 drops by two orders of magnitude.[61] Besides, Colussi proposed that HO•, consequently H_2O_2, are formed when partially hydrated HO^- and H^+ ions at the surface of colliding charged microdroplets undergo exothermic electron transfer.[67] The Head-Gordon group provided theoretical supports to the role of electric field, partial solvation, and charges in microdroplet H_2O_2 chemistry.[65-66]

Several theoretical and computational works have shown the presence of large IEFs at the air-water interface

localized to a region of several Angstroms at the surface.[34, 69-70] If these fields exist in real microdroplets, do they actually play a role in catalytic reactions? Furthermore, it remains unclear if the role of IEFs depend on the specific type of chemical reaction being studied. The current study aims to investigate and clarify the impact of the multiple factors, including specifically IEFs, potentially affecting the catalysis at or nearby to the water microdroplets surface where we focus on a typical Diels-Alder (DA) reaction.

The DA cycloaddition reaction represents one of the most important organic chemical reactions since its discovery in 1928 and it is widely used in the total synthesis of complex products.[71-74] While a past study indicated that the DA reaction is less favoured over other side-reaction(s) in water microdroplets,[75] exceptions are noted in the literature with the use of strained multi-cyclic hydrocarbon[76] or 'quasi-benzyne' intermediate.[77] This highlights the need to broaden the scope of DA reactions in microdroplets by investigating the factors that either facilitate, inhibit, or have no effect on their occurrence. In addition, the Coote group reported electrostatic catalysis of DA reaction using scanning tunnelling microscopy (STM),[78] providing experimental evidence that the reaction is accelerated by an external electric field. The sprayed microdroplets are rapidly evaporating and/or undergoing fission events. In these cases, the droplet interface is highly chaotic, so the electric field on the microdroplets may dynamically fluctuate, a situation that is quite different to that of the oriented static electric field generated by STM apparatus. This aspect further drives us to explore whether the spontaneous electric field present in microdroplets can affect the kinetics of DA reactions.

Herein, we combined first principles simulations and experiments to investigate the factors influencing a model DA reaction (Scheme 1) between cyclopentadiene (CPD) and acrylonitrile (ALT) in water microdroplets to examine the impact of the factors laid out above, with a special focus on IEF and partial solvation.

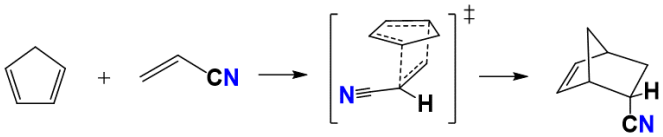

Scheme1. Diels-Alder reaction between cyclopentadiene (CPD) and acrylonitrile (ALT).

Our simulations predict that the cumulative effect of partial solvation and IEF cannot promote the DA reaction in water microdroplets. In fact, the barrier of the modeled DA reaction is higher at the air-water interface than in the bulk and this barrier is only slightly lowered under uniform external electric fields. Moreover, the IEF at the surface of water microdroplet is found to fluctuate continuously, a circumstance mitigating the overall electrostatic catalytic capability carried by the field. Microdroplet experiments with water and acetonitrile independently affirm these predictions and find instead that confinement effect and the increased concentration driven by evaporation are the key factors that increase the rate of the DA reaction in microdroplets. We would like to point out that the "confinement" in microdroplets, unlike the nanoconfinement, where length scales approach molecular dimensions, it refers to microconfinement, where the compartment dimensions encapsulate a relatively large number of solute molecules. This confinement limits the Brownian dynamics of reactants, thereby enhancing the frequency of bimolecular collisions necessary for reactions, be it on the surface or in the core. Recently, Wilson et al. introduced the term "kinetic confinement" to describe this effect in microdroplet reactions.[46]

This work elucidates the nuanced role of microdroplet interfaces in chemical reactivity, offering insights into optimizing reaction conditions for potential synthetic applications.

METHODOLOGY

Ab Initio Molecular Dynamics (AIMD) and Metadynamics (MetD) Simulations

To explicitly account for the effects carried by partial solvation on the DA reaction, we performed Born–Oppenheimer AIMD simulations combined with a well-tempered MetD approach using the CP2K package.[79-80] Simulations started from the reactant complex (RC) state, and aimed at determining the free-energy barriers of the reaction in the gas phase, at the air-water interface, and in the bulk. As for the simulation in the gas phase and in the bulk, the cubic box size was 12 Å × 12 Å × 12 Å. The bulk model includes 52 water molecules and one reactant (i.e., CPD+ALT). As far as the AIMD+MetD simulations of the water interface are concerned, water slabs containing up to 200 water molecules were constructed (Figure S1).

Both simulations in the bulk and at the interface were preliminarily equilibrated for at least 5 ps keeping the RC fixed whereas water molecules were allowed to relax. All AIMD+MetD simulations were conducted employing the dispersion-corrected BLYP-D3 exchange and correlation functional with DZVP-MOLOPT-SR-GTH basis set.[81-84] The energy cutoff was set to 400 Ry. The self-consistent field cycle was converged using the orbital transformation method. The dynamics of the system was simulated classically within the NVT ensemble with a timestep of 1 fs. The average temperature was controlled at 300 K using a Nose–Hoover thermostat chain with a coupling time constant of 50 fs. The distances between two pairs of C-C atoms, i.e. C1-C4 and C2-C3 distances, were selected as the collective variables (CVs) for this study (Figure 1). Additionally, block average analysis was performed on the calculated free-energy barriers and on the chosen CVs of the TSs for all the investigated systems to estimate the associated error bars. A more detailed description along with additional results of all the AIMD+MetD simulations can be found in the Supporting Information.

Density Functional Theory (DFT) Calculations. DFT calculations were performed using the Gaussian16 software package.[85] The M06-2X hybrid meta-GGA functional in combination with a 6-311++G(d,p) basis set was used.[86-87] A

benchmark preliminary investigation is provided in the Supporting Information (Table S1) to validate the choice of this level of theory. An implicit solvent polarizable continuum model (PCM) was used to model the aqueous phase. Vibrational frequencies were calculated to confirm the nature of all stationary points found and to ascertain that potential energy minima have no imaginary frequencies whilst transition states (TSs) exhibit only one imaginary frequency. Intrinsic reaction coordinate (IRC) calculations were performed on each TS to identify the minimum energy path in this kind of calculation.

The effects produced by static and homogeneous external electric fields (EEFs) were studied using the "Field = M ± N" keyword in Gaussian 16, where M defines the axis of the EEF, ± the direction of the field along the axis, and N its magnitude. EEF strengths in the range [−0.1; +0.1] V/Å were explored. EEFs were applied along the direction of formation of the C-C bond, which we aligned along the Z-axis of our reference system, and along orthogonal directions, namely X, and Y (Figure 1).

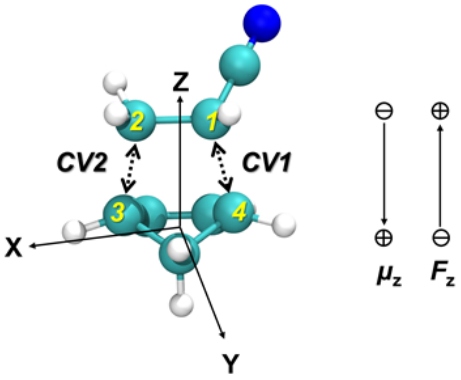

Figure 1. Representations of the reference system adopted for describing the DA reaction between cyclopentadiene (bottom) and acrylonitrile (top) along with the chosen collective variables (CV1 and CV2). Right panel defines the direction of the dipole moment (μ_z) and the external electric field (F_z) along z-axis.

RESULTS AND DISCUSSION

Effects of partial solvation. The free-energy landscapes of the DA reaction between cyclopentadiene (CPD) and acrylonitrile (ALT) to form endo-type product were computed for the reaction in the bulk (Figure 2a), at air-water interface (Figure 2b), and in gas phase (Figure S2) by performing AIMD+MetD simulations. The reaction proceeds through a pre-reaction complex (RC) and a transition state (TS) before forming the product (P) (Figure 2c). The computed internal free-energy barrier $\Delta G^{\ddagger}_{int}$, which equals G(TS) – G(RC), increases from 18.2 kcal/mol in the bulk to 19.2 kcal/mol at the air-water interface, and to 20.7 kcal/mol in the gas phase. This trend of an increasing barrier from bulk to the gas phase agrees rather well with our DFT calculations performed at a higher theory level (Figure S13). The observation that the free-energy barrier associated with the reaction occurring at the interface being slightly higher than its bulk counterpart is consistent to previous works.[88-89]

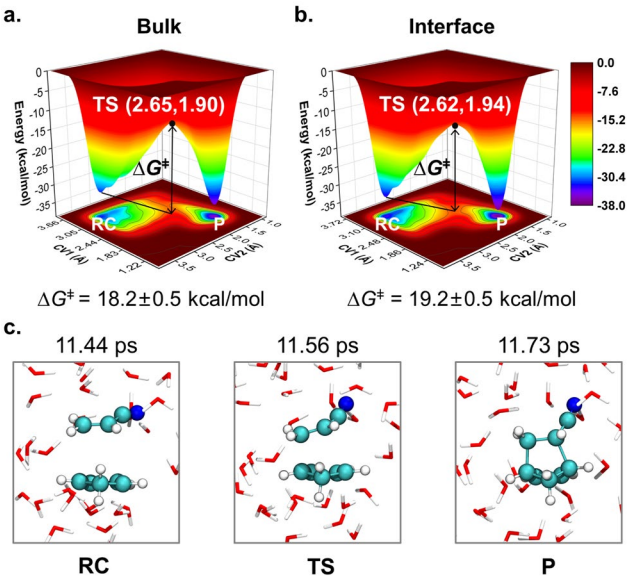

Figure 2. Free-energy landscape of the DA reaction between cyclopentadiene and acrylonitrile (a) in bulk water and (b) at the air-water interface as computed from AIMD+MetD simulations. (c) Snapshots of the RC, TS, and P structures in the simulation of the bulk system. Method: BLYP-D3/DZVP-MOLOPT-SR-GTH.

We attribute the free-energy barrier difference between the air-water interface case and the bulk one to the different stabilization modalities of the RC and TSs. To prove this hypothesis, we have analysed the structures and computed the average number of hydrogen bonds (HBs), n_{HB}, between the N-atom in ALT and the H-atom in water molecules surrounding RC and TS.[88, 90] In the bulk solution, n_{HB} equals to 1.67 and 2.10 for RC and TS, respectively. At the air-water interface, instead, the respective values decrease to 1.48 and 1.82. In comparison, as the system transits from the bulk to the interface, the number of HBs surrounding the TS decreases more than that for the RC, indicating that the TS is destabilized more than the RC as a result of solvent molecule loss. This differential destabilization effect leads to a higher free-energy barrier at the interface. This observation aligns with previous findings.[88, 91-92]

In a nutshell, our simulations indicate the barrier of DA reaction with a partially solvated state at the interface increases with respect to the bulk, so the partial solvation effect cannot be the source for the acceleration of the DA reaction in water microdroplets.

It is known that electric fields (EFs) can affect the reaction kinetics.[78, 93-100] Notably, unlike the EFs at charged tips/electrodes which are directional, the interfacial electric field (IEF) at the surface of a water microdroplet continuously fluctuates over time. Hence, we first computed the barrier change under static and homogeneous external electric fields (EEF) applied along different directions, including the one coinciding with the reaction axis, to gain an upper limit of the catalytic effect on the DA reaction, then we examined the effect of the spontaneously fluctuating IEFs at the air-water interface.

Effect of external electric field (EEF). To quantify the impact of EEFs on the DA reaction, we conducted a series of quantum-mechanical calculations where we first applied a uniform static and homogeneous EEF, F, to both the RC and TS along the X, Y, and Z directions, as defined in Figure 1. F_z is aligned along the reaction axis, corresponding to the direction along which the new C–C bonds are forming, whereas F_X/F_Y are aligned perpendicularly to the reaction axis. Molecular structures were optimized under the action of the applied EEF and the resulting energetics are listed in Table 1. It is observed that only applying a positive F_Z lowers the energy barrier, whereas the application of F_X and F_Y raises the height of the barrier. This is consistent with the "reaction-axis rule" proposed by Shaik,[97, 101-102] which states that the application of an EEF along the reaction axis (F_Z here) lowers the barrier, whilst F_X/F_Y induce selectivity between endo- and exo-cycloadducts. Since we are interested in ascertaining the catalytic role of the EEF, we will focus on the results emerging from the application of F_Z only.

Table 1. Calculated potential energy barriers of the DA reaction between CPD and ALT in aqueous (implicit solvation model) and gas phase under static external electric fields (EEFs) of various strengths. Method: M06-2X/6-311++G(d,p).

	$\Delta G^{\ddagger}$ (kcal/mol)					
	Aqueous			Gas		
EEF(V/Å)	F_x	F_y	F_z	F_x	F_y	F_z
0.1	21.7	23.6	17.8	21.8	23.8	20.0
0.05	21.1	20.8	18.5	21.2	21.1	20.1
0	20.0	20.0	20.0	20.8	20.8	20.8
-0.05	20.4	20.0	20.7	20.5	20.9	21.3
-0.1	20.9	20.3	21.8	20.9	21.2	22.0

Figure 3a shows that applying F_z in the positive direction lowers the barrier, whereas in the negative direction it raises the barrier, evidencing that EEFs on the z-axis have either significant catalytic or inhibitory effects on the DA reaction in both gas and aqueous phases.[101] Tracking the energy change of the stationary points (Figure S14) indicates that a positive F_z stabilizes the TS more than the RC, and this different stabilization leads to the barrier decrease. The different response of TS and RC to the EEF aligns with the fact that the Z-component of the dipole moment, μ_Z, is larger for the TS (2.26 D in gas, 3.03 D in aqueous phase) than for the RC (-0.36 D in gas, -0.54 D in aqueous phase). It is known that in the presence of a uniform EEF F_Z, the change in free energy G of a molecular system is approximately $\Delta G = -\mu_{Z,0}F_Z$.[103] Hence, the barrier change subjected to the EEF is $\Delta\Delta G^{\ddagger} = \Delta\mu_{Z,0}^{\ddagger}F_Z$. As shown in Figure 3a, the barrier decrease in presence of F_Z is faster in the aqueous than in the gas phase. This can be explained by the different $\Delta\mu_{Z,0}$ values: 2.62 D in the gas phase and 3.57 D in the liquid.

Inspection of the TS indicates that applying a positive F_Z polarizes the TS structure and hence enhances its asynchronicity. In the aqueous phase, as F_z increases from 0 to 0.1 V/Å, μ_Z of the TS increases from 3.03 D to 4.02 D, because a larger electron density fraction is transferred from the CPD-moiety to the ALT-moiety, where the Mulliken charge of the latter changes from -0.25 e to -0.29 e (Figure S15). At the same time, the C1-C4 bond distance (denoted as CV1) increases and the C2-C3 bond distance (denoted as CV2) decreases. Their difference, $\Delta CV = CV1\text{-}CV2$, is defined as the asynchronicity of the TS. As a result, ΔCV increases from 0.30 Å under field-free condition to 0.33 Å under F_z = 0.1 V/Å. These observations are in line with the work of Bickelhaupt and Shaik groups.[101, 104]

When F_Z=0.1 V/Å, the above calculation leads to a barrier drop of 2.2 kcal/mol compared to the field-free condition in the aqueous phase modeled with implicit solvation. To account for the solute-solvent interaction, we further performed AIMD simulations in combination with well-tempered MetD with explicit solvent molecules under a 0.1 V/Å static EEF. Simulation details are present in the Supporting Information. After the application of the EEF, there is a noticeable change in the overall orientation of the water molecules. This can be clearly observed from the snapshots reported in Figure S10 where, compared to the field-free condition, the orientation of water molecules becomes more ordered under the field action. During the simulation, the angle between the EEF and the reactants dipole moment is maintained in a range between 20° and 80° (Figure 3b), an arrangement facilitating the charge transfer from CPD to ALT.

The simulated free-energy barrier changes from 18.2 kcal/mol under field-free condition to 15.8 kcal/mol under a 0.1 V/Å field, leading to a drop of 2.4 kcal/mol (Figure S3), close to the value (2.2 kcal/mol) predicted using an implicit solvent model. This corresponds to roughly 50 times increase in the rate constant using Eyring-Polanyi equation. Committor analysis confirms that the asynchronicity of the TS with explicit solvent molecules also increases under the EEF (Figure S11), where ΔCV increases from 0.75 Å in the zero-field condition to 0.89 Å under F_z = 0.1 V/Å.

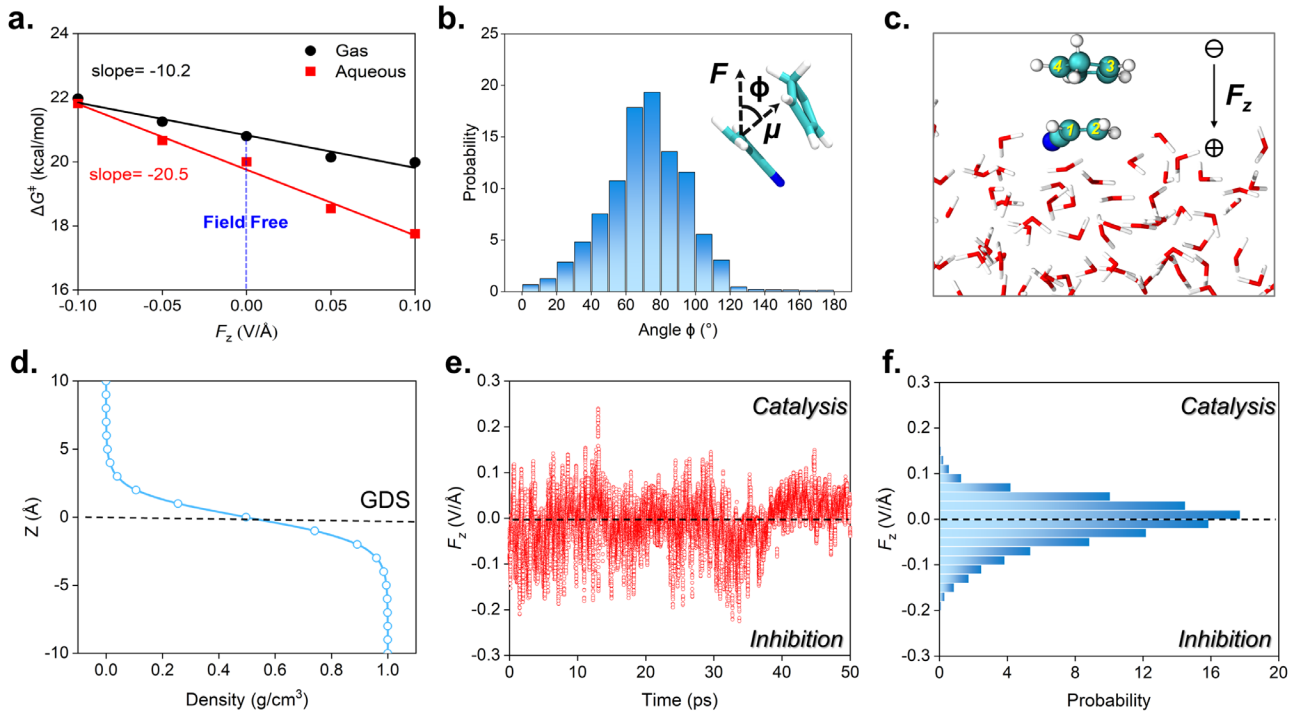

Figure 3. (a) Change of $\Delta G^{\ddagger}$ of DA reaction between CPD and ALT as a function of uniform external electric field F_z in gas (black dots) and aqueous (red squares) phase. (b) Distribution of the angle (ϕ) between the electric field and reactants dipole moment during a simulated trajectory under an external electric field of 0.1 V/Å applied along the z-axis from AIMD+MetD simulations. (c) Model for calculating the electric field generated by interfacial water molecules. (d) Water density profiles from the unbiased AIMD simulation, with the black line marking the Gibbs dividing surface (GDS). (e) Electric field generated by the interfacial water molecules along the z-axis as a function of time from the unbiased AIMD simulation. (f) Statistical distribution of the electric field generated by interfacial water molecules.

Effect of intrinsic interfacial electric field (IEF). The simulations presented above give an upper limit of the free-energy barrier change when a possible EF of water microdroplet is perfectly aligned along the reaction coordinate of a given chemical reaction. However, microdroplet interfaces are strongly dynamic entities, making rapidly fluctuating the orientation and magnitude of the IEF, thus affecting its putative catalytic properties. To shed light on this aspect of pivotal concern, we performed unbiased AIMD simulations (i.e., no MetD) to evaluate the genuine distribution of the IEF at the air-water interface by computing the IEF generated by interfacial water molecules along the z-axis of the DA reaction. To do so, we constructed an air-water interface model with 200 water molecules and placed the RC at the interface (Figure S1). The system was simulated for 50 ps, during which the RC was kept fixed while the water molecules were allowed to evolve dynamically by first principles at finite temperature.

Figure 3c shows a snapshot of the AIMD simulation of the RC at the air-water interface and Figure 3d shows the water density profile. The electrostatic potential generated by the Mulliken charges of the water molecules within the interfacial region on RC has been calculated. Specifically, we consider the solvent EF, *F*, calculated at the C1 atom position of RC and oriented along the Z-axis (i.e., reaction axis). The direction of such a Cartesian component is defined in the same way as in Figure 2a, so that a positive value promotes the DA reaction. Computing details are provided in the Supporting Information. Figure 3e depicts that the IEF generated by interfacial water molecules along the reaction axis fluctuates between -0.2 and 0.2 V/Å, with the majority falling within the range of -0.1 to 0.1 V/Å. It is noteworthy that also additional simulations without fixing the RC were performed, leading to similar results (Figure S12). The dynamic nature of the air-water interface and the fluctuating character of the IEF was previously reported also by the M. F. Ruiz-López group where they used an OH radical as a probe,[105] as well as the T. Head-Gordon group where the IEF was projected onto the O-H bond of a water molecule.[34] According to the 50-ps-long AIMD simulation we report in this work, the resulting time average of the IEF is -0.007 ± 0.0002 V/Å. If we plug this value into the formula $\Delta\Delta G^{\ddagger} = -\Delta\mu_{Z,0}{}^{\ddagger} F_Z$, and let the value of $\Delta\mu_{Z,0}$ to be 3.1 D, which is the average of the DFT value calculated above in the gas phase (2.62 D) and in aqueous phase (3.57 D, implicit solvent model), it leads to a barrier increase of only ~ 0.02 kcal/mol. Based on this small average value, one might be tempted to conclude that the electrostatic solvation effects on chemical reactivity are negligible. This, however, should be interpreted with caution because the average value masks the potential role of fluctuations and dynamical effects. Local IEF may have chances to catalyze the reaction when properly oriented along the reaction axis, as represented in the upper half of Figure 3e, f. Nevertheless, the catalytic capability of the IEF

might not be as effective as applied spatially and temporarily uniform EEFs since IEFs continuously change both in magnitude and direction as time evolves. Although the strengths of the EF found on microdroplets surfaces reported in the literature span several orders of magnitude, ranging from 10^5 to 10^9 V/m,[32-36, 106], the fact that the larger fields used in the current work (i.e., 10^9 V/m) are not capable to dramatically modify the free energy landscape of the DA reaction suggests that orders of magnitude lower fields have negligible effects on its catalysis.

Taken together, the aforementioned simulations indicate that 1) partial solvation at air-water interface increases the barrier of the DA reaction between ALT and CPD (Scheme 1) by about 1 kcal/mol relative to the bulk; 2) an applied static and homogeneous EEF of 0.1 V/Å is capable of lowering its barrier by about 2 kcal/mol only if oriented along the reaction axis; 3) the air-water IEF fluctuates continuously, rendering its catalytic capability limited as compared to the constant and uniform EEF case. Therefore, the cumulative effect of the partial solvation and IEF does not appear to promote the DA reaction between cyclopentadiene and acrylonitrile in water microdroplets. If, however, this DA reaction was to be accelerated in water microdroplets, other factors should be responsible.

To validate our computational predictions, a series of experimental investigations were conducted, which are reported in the following section, which confirm that IEF and partial solvation are not important factors to drive this reaction in microdroplets. Instead, enrichment of reactants in confined volumes driven by fast evaporation becomes predominant. This factor has been identified to be responsible for the acceleration of many reactions in the works of Cooks, Wilson, and Williams.[46, 48, 51, 53, 107-110]

Mass spectrometry experiment. In the bulk phase, the above DA reaction is known to occur in the presence of a heterogeneous catalyst at an elevated temperature.[111] Cyclopentadiene is highly reactive and undergoes a self-DA reaction, forming dicyclopentadiene. Therefore, we used dicyclopentadiene in our microdroplet experiment, which spontaneously undergoes a retro-DA reaction within the droplet to produce cyclopentadiene (vide infra).[112] We separately prepared two solutions by mixing dicyclopentadiene and acrylonitrile, each with 200 μM concentration, in water and acetonitrile for comparison, followed by atomizing those solutions immediately using a home-built sonic spray source in front of a mass spectrometer inlet (Figure 4a). Unless otherwise stated, the spray source was operated without applying any voltage under a 120-psi nebulizing gas (nitrogen) pressure at a distance of 15 mm from the MS inlet capillary, following a 10 μL/min and 50 μL/min flow rates of water and acetonitrile solutions, respectively, to ensure the recording of ion signals from species at sufficient intensities.

Figure 4b schematically presents the MS detection of different intermediates and products from dicyclopentadiene (**R1**) and acrylonitrile (**R3**) reactions in water or acetonitrile microdroplets (Table S6). In water microdroplets, the dominant reaction was oxidation, forming the ketone **Ox1** from **R1** and ketone **Ox2** from **R2,** as recorded in the corresponding mass spectrum (Figure 4c). These ketones

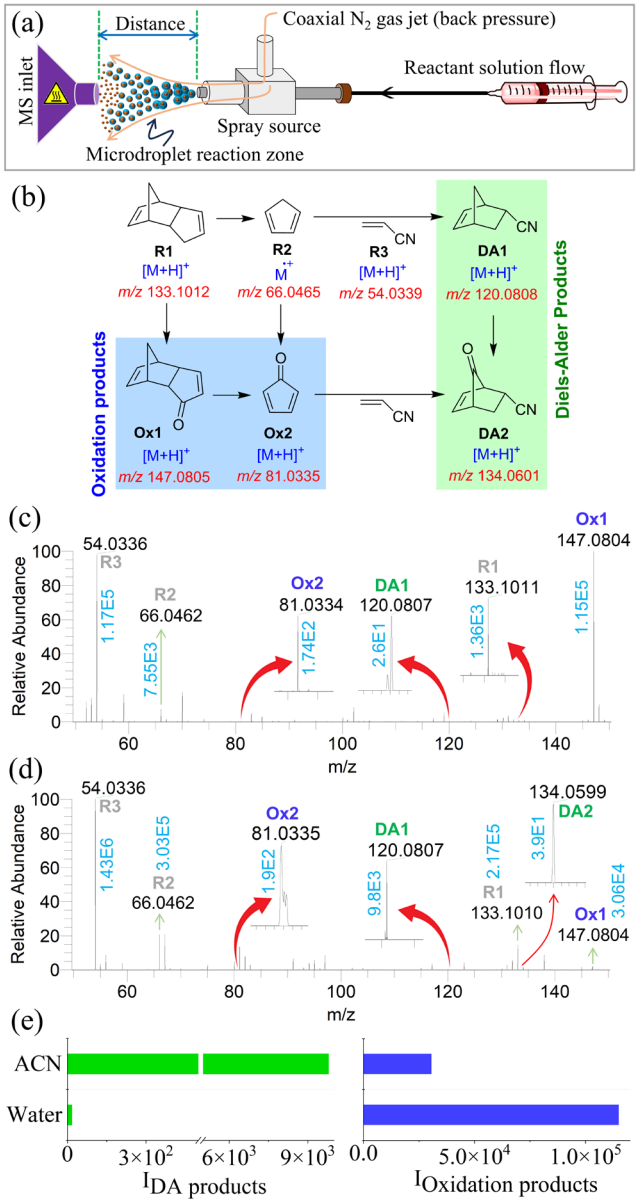

Figure 4. (a) Diagram of the experimental setup for mass spectrometric monitoring of the reaction of dicyclopentadiene and acrylonitrile in microdroplets obtained from a sonic spray source. (b) Schematic presentation of the dual pathways leading to DA and oxidation products in microdroplets as evaluated by MS. The theoretical m/z values of the charged species are indicated below the corresponding structures. The sonic spray (under 0V) mass spectra obtained from spraying a mixture of dicyclopentadiene and acrylonitrile in (c) water and (d) acetonitrile (ACN). The cyan numerical values denote the absolute intensity of the corresponding peak. (e) Histograms showing the screening of the two spray solvents to track the sum of the ion intensities for the DA products (left panel) and oxidation products (right panel), as recorded in the respective mass spectra.

were also characterized by tandem mass spectrometry (Figure S18). However, only a minor extent of the DA reaction,

relative to oxidation, was observed in the water microdroplets, as evidenced by detecting a trace level of the product **DA1**. Assuming similar ionization efficiencies for the nitrile compounds (**R3** and **DA1**), the intensity values of these species in the mass spectral data (Figure 4c) indicate that the yield of the DA reaction in water microdroplets is approximately 0.02%. However, the acetonitrile microdroplets were more effective in facilitating the DA reaction, yielding two products (**DA1** and **DA2**) with a combined yield of approximately 0.7% (Figure 4d). Given that the average droplet lifetime is around a few hundred microseconds (see Section III in supporting information), these yields, albeit lower in quantity, suggest a more than 10^6-fold increase of the DA reaction rate in both water and acetonitrile microdroplets compared to the corresponding bulk phase, where the reported rate constant is in the order of 10^{-5} $M^{-1}s^{-1}$.[113] (see Section III in Supporting Information).

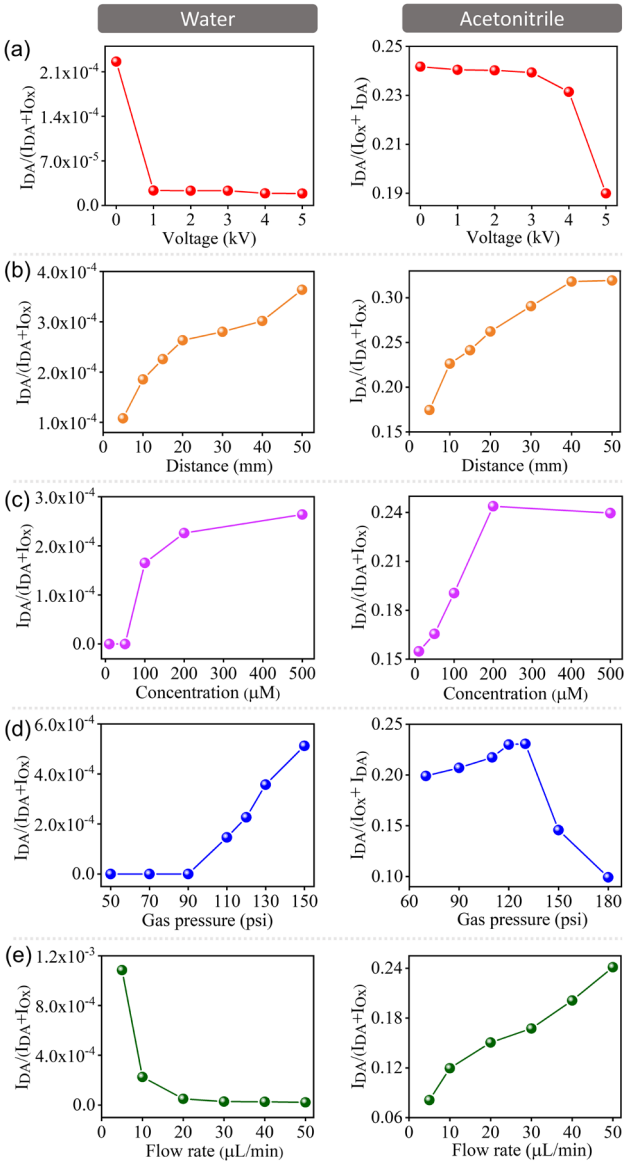

Figure 5. Evaluating the fractional abundance of Diels-Alder (DA) products across all DA and oxidation products in water (left column) and acetonitrile (right column) microdroplets on tuning various spray parameters: (a) spray voltage, (b) distance between spray tip to MS inlet (c) reactant concentration, (d) nebulizing gas pressure, and (e) solution flow rate. The fractional abundance of DA products was calculated using the formula $I_{DA}/(I_{DA}+I_{Ox})$, where I_{DA} represents the sum of the intensities of the DA products, and I_{Ox} denotes the sum of the intensities of the oxidation products.

Although oxidation reactions predominated over DA reactions in both water and acetonitrile droplets (Figures 4c-d), oxidation efficiency was significantly lower in acetonitrile droplets compared to water droplets. This result suggests that microdroplet-generated hydroxyl radicals or reactive oxygen species may play a key role in driving the oxidation of alkane (**R1** and **R2**) to ketone.[10, 12-13, 16, 18, 36, 57] A trace amount of water as an impurity in acetonitrile, or the exposure of the acetonitrile droplets to moisture in the air might have driven the observed oxidation reaction (Figure 4d). Figure 4e presents the histogram compiling the above results, showing that oxidation occurred effectively in water droplets, while the DA reaction was relatively more prominent in acetonitrile droplets. To explore the reasons behind these differences and identify factors that might influence the DA reactions in microdroplets, we assessed the reactions under various spray conditions.

We measured the fractional abundance of DA products across all products (**Ox1**, **Ox2**, **DA1**, and **DA2**) in the mass spectra recorded by tuning the spray parameters. Microdroplets formed using a 0V spray (see Figure 4) typically carry net charges, mostly attributed to the statistical fluctuations of ions like H^+ and OH^- during the gas-assisted atomization of water.[35, 106, 114-115] Earlier reports demonstrated that when a spray potential is applied, there is a dramatic increase in droplet charging (>100-fold),[39] likely facilitated by the solvent redox process (electrospray charging). Therefore, when we gradually increased the spray potential to +5 kV, producing highly charged microdroplets, this likely intensified the IEF due to an increased net surface charge. Subsequently, we observed a significant reduction in the extent of the DA reaction in water droplets as compared to those in acetonitrile droplets (Figure 5a). This result indicates a marked preference for oxidation reactions at the charged surface of water microdroplets at the expense of the competing DA reactions (Figure S19), which may not prefer the charged environment of the droplet and, hence, the associated EF at the surface. In other words, the IEF has a negligible role in promoting the DA reactions, as predicted by our simulations using both water and acetonitrile as solvent (Table S4). Instead, the IEF triggers oxidation reactions.

As increasing the distance between the spray source and the MS inlet increases the microdroplet reaction time and reduces the droplet size by its evolution (evaporation/fission) process, we tuned this distance to monitor its effect on the microdroplet reaction. Surprisingly, the increased flight time and subsequent evaporation of the microdroplets (Figure S20a) led to a higher fractional abundance of DA products (Figure 5b). This result suggests that

the trace level of the DA reaction observed in water microdroplets is possibly caused by the confinement or increased concentration of reactants in a small volume during the microdroplet evolution. Indeed, when we gradually increased the reactant concentration in microdroplets, the efficacy of the DA reaction improved (Figure 5c). The increased nebulizing gas pressure in the spray source is known to cause faster droplet solvent evaporation (Figure S20b) and fission, producing smaller droplets with a high surface-to-volume ratio.[116-117] When we raised the gas pressure, the tendency of the DA reaction in water microdroplets continued to increase (Figure 5d). This suggests that the DA reaction might predominantly occur at the air-water interface, facilitated by the accumulation (increased concentration) of hydrophobic reactants at that location. The acetonitrile droplet also exhibited a similar reaction trend up to a certain gas pressure (130 psi), after which the propensity of DA reaction decreased (Figure 5d). This result might be explained by the possible distribution of hydrophobic reactants throughout the acetonitrile droplet, allowing the DA reaction to occur both at the interface and within the core of the acetonitrile droplet, which is in contrast to the water droplet case as discussed above.

However, the oxidation reaction in either acetonitrile or water droplets is expected to occur primarily at the droplet surface, where reactive oxygen species are more prevalent. The rapid evaporation of acetonitrile results in a substantial increase in the surface-to-volume ratio of acetonitrile microdroplets at elevated nebulizing gas pressures (>130 psi), promoting oxidation reactions at the expense of DA reactions at the interface. This hypothesis is supported by studies investigating the impact of varying spray solution flow rates on the reactions (Figure 5e). Ramping up the flow rate of the spray solution leads to larger microdroplets with a decreased surface-to-volume ratio (Figure S20c). As both DA and oxidation reactions are expected to occur at the surface of water microdroplets, the efficacy of both these reactions decreased with the increase in the aqueous solution flow rate. However, the DA reaction experienced a more pronounced decrease than the oxidation reaction, reducing the fractional abundance of DA products with an increasing flow rate (Figure 5e). This result again points to the effect of polar water on enhancing the local concentration of hydrophobic reagents at the air-water interface to impart the DA reaction, albeit with a lower propensity compared to the dominant oxidation reactions. In contrast, the impact of the acetonitrile flow rate on the DA reaction was different, i.e., the fractional abundance of DA products increased by increasing the flow rate (Figure 5d). This result indicates that the DA reaction in acetonitrile microdroplets is not restricted solely to its surface but predominantly extends throughout its core. The increased solution mass flow supplied a greater quantity of reagents per droplet, and due to the rapid evaporation of acetonitrile, the droplet became enriched with reagents confined in a small space, which subsequently impacted the DA reaction inside the acetonitrile droplet.

CONCLUSIONS

By the means of a series of simulation approaches and experimental investigations, we explore the acceleration phenomenon (i.e., catalysis) of a Diels-Alder (DA) reaction between cyclopentadiene and acrylonitrile in water microdroplets. Quantum-mechanical calculations and first-principles molecular dynamics coupled with enhanced sampling techniques revealed that the partial solvation effect and local interfacial electric field at the water microdroplet surface are not factors accelerating the DA reaction. Specifically, the free-energy barrier of the DA reaction at the water microdroplet interface was found to be approximately 1 kcal/mol higher compared to the bulk phase one. Although the presence of a local strong electric field at the gas-liquid interface could slightly decrease the barrier by about 2 kcal/mol along the reaction axis, the fluctuating nature of this interfacial electric field significantly inhibits its catalytic effect on the DA reaction. These predictions were confirmed by microdroplet experiments.

Experimentally, the DA reaction is not as highly favored as oxidation reactions in water microdroplets. However, the detection of trace levels (0.02%) of DA products from the reaction between dicyclopentadiene and acrylonitrile in water microdroplets is attributed to the surface enrichment of these hydrophobic reactants on the droplet surface. The increased polarity (or charge) or electric field on such droplet surfaces inhibits the DA reaction by promoting substrate oxidation, indicating that the local electric field does not facilitate the DA reaction at the air-water interface. Additionally, the study, dependent on spray parameters, revealed that while the DA reaction might occur at the surface of water microdroplets, it prefers to occur within the core of acetonitrile droplets, suggesting that partial solvation is not necessarily a critical factor for this reaction. Instead, the rapid evaporation of microdroplets and the subsequent reagent enrichment within the accessible confined volume of microdroplets are the driving force for acceleration of the DA reaction in microdroplets. We also emphasize that the conclusions drawn above are based on a single DA reaction and may not necessarily apply universally to other reactions, as the specific factors accelerating each reaction type can vary. Overall, the reactivity enhancement in microdroplet is a result of multiple factors working in concert, and our combined computational and experimental efforts are dedicated to dissecting the contribution of each factor to such a model reaction. However, further research is expected to provide better insights into these aspects in the next future. This work provides insights for manipulating reactions in water microdroplets, offering potential perspectives on leveraging water microdroplet chemistry for future applications.

ASSOCIATED CONTENT

Supporting Information.
Experimental and theoretical methods, supplementary experimental and theoretical results, and computational raw data. This material is available free of charge via the Internet at http://pubs.acs.org.

Notes
The authors declare no competing financial interests.

ACKNOWLEDGMENT

J.X. acknowledges financial support from the National Natural Science Foundation of China (no. 22273004), Beijing Natural Science Foundation (no. 2222028), and the Teli Fellowship from Beijing Institute of Technology, China. S.B. acknowledged support from Science and Engineering Research Board, India (grant number CRG/2022/002676). G.C. acknowledges financial support from ICSC – Centro Nazionale di Ricerca in High-Performance Computing, Big Data and Quantum Computing, funded by European Union – NextGenerationEU - PNRR, Missione 4 Componente 2 Investimento 1.4. G.C. acknowledges the European Union – NextGeneration EU from the Italian Ministry of Environment and Energy Security POR H2 AdP MMES/ENEA with involvement of CNR and RSE, PNRR - Mission 2, Component 2, Investment 3.5 "Ricerca e sviluppo sull'idrogeno", CUP: B93C22000630006. G.C. acknowledges the European Union (NextGeneration EU), through the MUR-PNRR project SAMOTHRACE (ECS00000022). G.C. is thankful to CINECA for awards under the ISCRA initiative for the availability of high-performance computing resources and support. A. H. also acknowledges funding by the European Union (ERC, HyBOP, Grant Number: 101043272). Views and opinions expressed are however those of the author(s) only and do not necessarily reflect those of the European Union or the European Research Council. Neither the European Union nor the granting authority can be held responsible for them. The authors thank Prof. Michelle L. Coote for helpful discussions.

Author Contributions

[#]K.G. and N. A. contributed equally to this work.

Notes

The authors declare no competing financial interests.

REFERENCES

(1) Banerjee, S.; Zare, R. N., Syntheses of Isoquinoline and Substituted Quinolines in Charged Microdroplets. *Angew. Chem. Int. Ed.* **2015,** *54* (49), 14795-14799.
(2) Girod, M.; Moyano, E.; Campbell, D. I.; Cooks, R. G., Accelerated bimolecular reactions in microdroplets studied by desorption electrospray ionization mass spectrometry. *Chem. Sci.* **2011,** *2* (3), 501-510.
(3) Lai, Y.-H.; Sathyamoorthi, S.; Bain, R. M.; Zare, R. N., Microdroplets Accelerate Ring Opening of Epoxides. *J. Am. Soc. Mass Spectrom.* **2018,** *29* (5), 1036-1043.
(4) Lee, J. K.; Banerjee, S.; Nam, H. G.; Zare, R. N., Acceleration of reaction in charged microdroplets. *Q. Rev. Biophys.* **2015,** *48* (4), 437-444.
(5) Song, Z.; Liang, C.; Gong, K.; Zhao, S.; Yuan, X.; Zhang, X.; Xie, J., Harnessing the High Interfacial Electric Fields on Water Microdroplets to Accelerate Menshutkin Reactions. *J. Am. Chem. Soc.* **2023,** *145* (48), 26003-26008.
(6) Chen, H.; Wang, R.; Xu, J.; Yuan, X.; Zhang, D.; Zhu, Z.; Marshall, M.; Bowen, K.; Zhang, X., Spontaneous Reduction by One Electron on Water Microdroplets Facilitates Direct Carboxylation with CO_2. *J. Am. Chem. Soc.* **2023,** *145* (4), 2647-2652.
(7) Eremin, D. B.; Fokin, V. V., On-Water Selectivity Switch in Microdroplets in the 1,2,3-Triazole Synthesis from Bromoethenesulfonyl Fluoride. *J. Am. Chem. Soc.* **2021,** *143* (44), 18374-18379.
(8) Gnanamani, E.; Yan, X.; Zare, R. N., Chemoselective N-Alkylation of Indoles in Aqueous Microdroplets. *Angew. Chem. Int. Ed.* **2020,** *59* (8), 3069-3072.
(9) Holden, D. T.; Morato, N. M.; Cooks, R. G., Aqueous microdroplets enable abiotic synthesis and chain extension of unique peptide isomers from free amino acids. *Proc. Natl. Acad. Sci.* **2022,** *119* (42), e2212642119.
(10) Meng, Y.; Gnanamani, E.; Zare, R. N., Direct C(sp^3)–N Bond Formation between Toluene and Amine in Water Microdroplets. *J. Am. Chem. Soc.* **2022,** *144* (43), 19709-19713.
(11) Meng, Y.; Gnanamani, E.; Zare, R. N., One-Step Formation of Pharmaceuticals Having a Phenylacetic Acid Core Using Water Microdroplets. *J. Am. Chem. Soc.* **2023,** *145* (14), 7724-7728.
(12) Meng, Y.; Gnanamani, E.; Zare, R. N., Catalyst-Free Decarboxylative Amination of Carboxylic Acids in Water Microdroplets. *J. Am. Chem. Soc.* **2023,** *145* (1), 32-36.
(13) Meng, Y.; Zare, R. N.; Gnanamani, E., One-Step, Catalyst-Free Formation of Phenol from Benzoic Acid Using Water Microdroplets. *J. Am. Chem. Soc.* **2023,** *145* (35), 19202-19206.
(14) Nam, I.; Lee, J. K.; Nam, H. G.; Zare, R. N., Abiotic production of sugar phosphates and uridine ribonucleoside in aqueous microdroplets. *Proc. Natl. Acad. Sci.* **2017,** *114* (47), 12396-12400.
(15) Nandy, A.; Kumar, A.; Mondal, S.; Koner, D.; Banerjee, S., Spontaneous Generation of Aryl Carbocations from Phenols in Aqueous Microdroplets: Aromatic SN1 Reactions at the Air–Water Interface. *J. Am. Chem. Soc.* **2023,** *145* (29), 15674-15679.
(16) Song, X.; Basheer, C.; Xia, Y.; Li, J.; Abdulazeez, I.; Al-Saadi, A. A.; Mofidfar, M.; Suliman, M. A.; Zare, R. N., One-step Formation of Urea from Carbon Dioxide and Nitrogen Using Water Microdroplets. *J. Am. Chem. Soc.* **2023,** *145* (47), 25910-25916.
(17) Song, X.; Basheer, C.; Zare, R. N., Making ammonia from nitrogen and water microdroplets. *Proc. Natl. Acad. Sci.* **2023,** *120* (16), e2301206120.
(18) Song, X.; Meng, Y.; Zare, R. N., Spraying Water Microdroplets Containing 1,2,3-Triazole Converts Carbon Dioxide into Formic Acid. *J. Am. Chem. Soc.* **2022,** *144* (37), 16744-16748.
(19) Wang, T.; Li, Z.; Gao, H.; Hu, J.; Chen, H.-Y.; Xu, J.-J., Ultrafast C–C and C–N bond formation reactions in water microdroplets facilitated by the spontaneous generation of carbocations. *Chem. Sci.* **2023,** *14* (41), 11515-11520.
(20) Zhang, D.; Yuan, X.; Gong, C.; Zhang, X., High Electric Field on Water Microdroplets Catalyzes Spontaneous and Ultrafast Oxidative C–H/N–H Cross-Coupling. *J. Am. Chem. Soc.* **2022,** *144* (35), 16184-16190.
(21) Zhao, L.; Song, X.; Gong, C.; Zhang, D.; Wang, R.; Zare, R. N.; Zhang, X., Sprayed water microdroplets containing dissolved pyridine spontaneously generate pyridyl anions. *Proc. Natl. Acad. Sci.* **2022,** *119* (12), e2200991119.
(22) Zhu, C.; Pham, L. N.; Yuan, X.; Ouyang, H.; Coote, M. L.; Zhang, X., High Electric Fields on Water Microdroplets Catalyze Spontaneous and Fast Reactions in Halogen-Bond Complexes. *J. Am. Chem. Soc.* **2023,** *145* (39), 21207-21212.
(23) Nandy, A.; Mondal, S.; Koner, D.; Banerjee, S., Heavy Water Microdroplet Surface Enriches the Lighter Isotopologue Impurities. *J. Am. Chem. Soc.* **2024,** *146* (28), 19050-19058.
(24) Chen, X.; Xia, Y.; Zhang, Z.; Hua, L.; Jia, X.; Wang, F.; Zare, R. N., Hydrocarbon Degradation by Contact with Anoxic Water Microdroplets. *J. Am. Chem. Soc.* **2023,** *145* (39), 21538-21545.
(25) Gong, K.; Meng, Y.; Zare, R. N.; Xie, J., Molecular Mechanism for Converting Carbon Dioxide Surrounding Water Microdroplets Containing 1,2,3-Triazole to Formic Acid. *J. Am. Chem. Soc.* **2024,** *146* (12), 8576-8584.

(26) Jin, S.; Chen, H.; Yuan, X.; Xing, D.; Wang, R.; Zhao, L.; Zhang, D.; Gong, C.; Zhu, C.; Gao, X.; Chen, Y.; Zhang, X., The Spontaneous Electron-Mediated Redox Processes on Sprayed Water Microdroplets. *JACS Au* **2023,** *3* (6), 1563-1571.
(27) Gong, C.; Li, D.; Li, X.; Zhang, D.; Xing, D.; Zhao, L.; Yuan, X.; Zhang, X., Spontaneous Reduction-Induced Degradation of Viologen Compounds in Water Microdroplets and Its Inhibition by Host–Guest Complexation. *J. Am. Chem. Soc.* **2022,** *144* (8), 3510-3516.
(28) Yuan, X.; Zhang, D.; Liang, C.; Zhang, X., Spontaneous Reduction of Transition Metal Ions by One Electron in Water Microdroplets and the Atmospheric Implications. *J. Am. Chem. Soc.* **2023,** *145* (5), 2800-2805.
(29) Kumar, A.; Mondal, S.; Banerjee, S., Aqueous Microdroplets Capture Elusive Carbocations. *J. Am. Chem. Soc.* **2021,** *143* (6), 2459-2463.
(30) Kumar, A.; Mondal, S.; Mofidfar, M.; Zare, R. N.; Banerjee, S., Capturing Reactive Carbanions by Microdroplets. *J. Am. Chem. Soc.* **2022,** *144* (17), 7573-7577.
(31) Kumar, A.; Mondal, S.; Sandeep; Venugopalan, P.; Kumar, A.; Banerjee, S., Destabilized Carbocations Caged in Water Microdroplets: Isolation and Real-Time Detection of α-Carbonyl Cation Intermediates. *J. Am. Chem. Soc.* **2022,** *144* (8), 3347-3352.
(32) Chamberlayne, C. F.; Zare, R. N., Simple model for the electric field and spatial distribution of ions in a microdroplet. *J. Chem. Phys.* **2020,** *152* (18), 184702.
(33) Xiong, H.; Lee, J. K.; Zare, R. N.; Min, W., Strong electric field observed at the interface of aqueous microdroplets. *J. Phys. Chem. Lett.* **2020,** *11* (17), 7423-7428.
(34) Hao, H.; Leven, I.; Head-Gordon, T., Can electric fields drive chemistry for an aqueous microdroplet? *Nat. Commun.* **2022,** *13* (1), 280.
(35) Xia, Y.; Xu, J.; Li, J.; Chen, B.; Dai, Y.; Zare, R. N., Visualization of the Charging of Water Droplets Sprayed into Air. *J. Phys. Chem. A* **2024,** *128* (28), 5684-5690.
(36) Kumar, A.; Avadhani, V. S.; Nandy, A.; Mondal, S.; Pathak, B.; Pavuluri, V. K. N.; Avulapati, M. M.; Banerjee, S., Water Microdroplets in Air: A Hitherto Unnoticed Natural Source of Nitrogen Oxides. *Anal. Chem.* **2024,** *96* (26), 10515-10523.
(37) Qiu, L.; Wei, Z.; Nie, H.; Cooks, R. G., Reaction Acceleration Promoted by Partial Solvation at the Gas/Solution Interface. *ChemPlusChem* **2021,** *86* (10), 1362-1365.
(38) Wei, Z.; Li, Y.; Cooks, R. G.; Yan, X., Accelerated Reaction Kinetics in Microdroplets: Overview and Recent Developments. *Annu. Rev. Phys. Chem.* **2020,** *71* (1), 31-51.
(39) Banerjee, S., On the stability of carbocation in water microdroplets. *Int. J. Mass spectrom.* **2023,** *486*, 117024.
(40) Colussi, A. J.; Enami, S.; Ishizuka, S., Hydronium Ion Acidity Above and Below the Interface of Aqueous Microdroplets. *ACS Earth Space Chem.* **2021,** *5* (9), 2341-2346.
(41) Li, K.; Gong, K.; Liu, J.; Ohnoutek, L.; Ao, J.; Liu, Y.; Chen, X.; Xu, G.; Ruan, X.; Cheng, H.; Han, J.; Sui, G.; Ji, M.; Valev, V. K.; Zhang, L., Significantly accelerated photochemical and photocatalytic reactions in microdroplets. *Cell Rep. Phys. Sci.* **2022,** *3* (6), 100917.
(42) Li, M.; Kan, Y.; Su, H.; Pöschl, U.; Parekh, S. H.; Bonn, M.; Cheng, Y., Spatial homogeneity of pH in aerosol microdroplets. *Chem* **2023,** *9* (4), 1036-1046.
(43) Wei, H.; Vejerano, E. P.; Leng, W.; Huang, Q.; Willner, M. R.; Marr, L. C.; Vikesland, P. J., Aerosol microdroplets exhibit a stable pH gradient. *Proc. Natl. Acad. Sci.* **2018,** *115* (28), 7272-7277.
(44) Brown, E. K.; Rovelli, G.; Wilson, K. R., pH jump kinetics in colliding microdroplets: accelerated synthesis of azamonardine from dopamine and resorcinol. *Chem. Sci.* **2023,** *14* (23), 6430-6442.
(45) Feng, C.; Zhang, L., Microdroplet assisted hollow ZnCdS@PDA nanocages' synergistic confinement effect for promoting photocatalytic H_2O_2 production. *Mater. Horiz.* **2024,** *11* (6), 1515-1527.
(46) Wilson, K. R.; Prophet, A. M., Chemical Kinetics in Microdroplets. *Annu. Rev. Phys. Chem.* **2024,** *75*, 185-208.
(47) Briones, A. M.; Ervin, J. S.; Byrd, L. W.; Putnam, S. A.; White, A.; Jones, J. G., Evaporation Characteristics of Pinned Water Microdroplets. *J. Thermophys. Heat Transfer* **2012,** *26* (3), 480-493.
(48) Chen, C. J.; Williams, E. R., The role of analyte concentration in accelerated reaction rates in evaporating droplets. *Chem. Sci.* **2023,** *14* (18), 4704-4713.
(49) Marsh, B. M.; Iyer, K.; Cooks, R. G., Reaction Acceleration in Electrospray Droplets: Size, Distance, and Surfactant Effects. *J. Am. Soc. Mass Spectrom.* **2019,** *30* (10), 2022-2030.
(50) Putnam, S. A.; Briones, A. M.; Byrd, L. W.; Ervin, J. S.; Hanchak, M. S.; White, A.; Jones, J. G., Microdroplet evaporation on superheated surfaces. *Int. J. Heat Mass Transfer* **2012,** *55* (21), 5793-5807.
(51) Rovelli, G.; Jacobs, M. I.; Willis, M. D.; Rapf, R. J.; Prophet, A. M.; Wilson, K. R., A critical analysis of electrospray techniques for the determination of accelerated rates and mechanisms of chemical reactions in droplets. *Chem. Sci.* **2020,** *11* (48), 13026-13043.
(52) Enami, S.; Mishra, H.; Hoffmann, M. R.; Colussi, A. J., Protonation and Oligomerization of Gaseous Isoprene on Mildly Acidic Surfaces: Implications for Atmospheric Chemistry. *J. Phys. Chem. A* **2012,** *116* (24), 6027-6032.
(53) Gallo, A.; Farinha, A. S. F.; Dinis, M.; Emwas, A.-H.; Santana, A.; Nielsen, R. J.; Goddard, W. A.; Mishra, H., The chemical reactions in electrosprays of water do not always correspond to those at the pristine air–water interface. *Chem. Sci.* **2019,** *10* (9), 2566-2577.
(54) Colussi, A. J.; Enami, S., Comment on "The chemical reactions in electrosprays of water do not always correspond to those at the pristine air–water interface" by A. Gallo Jr, A. S. F. Farinha, M. Dinis, A.-H. Emwas, A. Santana, R. J. Nielsen, W. A. Goddard III and H. Mishra, Chem. Sci., 2019, 10, 2566. *Chem. Sci.* **2019,** *10* (35), 8253-8255.
(55) Gallo, A.; Farinha, A. S. F.; Emwas, A.-H.; Santana, A.; Nielsen, R. J.; Goddard, W. A.; Mishra, H., Reply to the 'Comment on "The chemical reactions in electrosprays of water do not always correspond to those at the pristine air–water interface"' by A. J. Colussi and S. Enami, Chem. Sci., 2019, 10, DOI: 10.1039/c9sc00991d. *Chem. Sci.* **2019,** *10* (35), 8256-8261.
(56) Jacobs, M. I.; Davis, R. D.; Rapf, R. J.; Wilson, K. R., Studying Chemistry in Micro-compartments by Separating Droplet Generation from Ionization. *J. Am. Soc. Mass Spectrom.* **2019,** *30* (2), 339-343.
(57) Gallo Jr, A.; Musskopf, N. H.; Liu, X.; Yang, Z.; Petry, J.; Zhang, P.; Thoroddsen, S.; Im, H.; Mishra, H., On the formation of hydrogen peroxide in water microdroplets. *Chem. Sci.* **2022,** *13* (9), 2574-2583.
(58) Mofidfar, M.; Mehrgardi, M. A.; Xia, Y.; Zare, R. N., Dependence on relative humidity in the formation of reactive oxygen species in water droplets. *Proc. Natl. Acad. Sci.* **2024,** *121* (12), e2315940121.
(59) Wang, S.; Yang, J.; Liu, F.; Xiao, S.; Xiao, F.; Dong, X.; Shan, S., Water microdroplets: A catalyst-free source of reactive oxygen species for pollutants removal. *J. Cleaner Prod.* **2023,** *420*, 138444.

(60) Xing, D.; Meng, Y.; Yuan, X.; Jin, S.; Song, X.; Zare, R. N.; Zhang, X., Capture of Hydroxyl Radicals by Hydronium Cations in Water Microdroplets. *Angew. Chem. Int. Ed.* **2022,** *61* (33), e202207587.
(61) Mehrgardi, M. A.; Mofidfar, M.; Zare, R. N., Sprayed Water Microdroplets Are Able to Generate Hydrogen Peroxide Spontaneously. *J. Am. Chem. Soc.* **2022,** *144* (17), 7606-7609.
(62) Angelaki, M.; Carreira Mendes Da Silva, Y.; Perrier, S.; George, C., Quantification and Mechanistic Investigation of the Spontaneous H_2O_2 Generation at the Interfaces of Salt-Containing Aqueous Droplets. *J. Am. Chem. Soc.* **2024,** *146* (12), 8327-8334.
(63) Musskopf, N. H.; Gallo, A.; Zhang, P.; Petry, J.; Mishra, H., The Air–Water Interface of Water Microdroplets Formed by Ultrasonication or Condensation Does Not Produce H_2O_2. *J. Phys. Chem. Lett.* **2021,** *12* (46), 11422-11429.
(64) Eatoo, M. A.; Mishra, H., Busting the myth of spontaneous formation of H_2O_2 at the air–water interface: contributions of the liquid–solid interface and dissolved oxygen exposed. *Chem. Sci.* **2024,** *15* (9), 3093-3103.
(65) Heindel, J. P.; Hao, H.; LaCour, R. A.; Head-Gordon, T., Spontaneous Formation of Hydrogen Peroxide in Water Microdroplets. *J. Phys. Chem. Lett.* **2022,** *13* (43), 10035-10041.
(66) Heindel, J. P.; LaCour, R. A.; Head-Gordon, T., The role of charge in microdroplet redox chemistry. *Nat. Commun.* **2024,** *15* (1), 3670.
(67) Colussi, A. J., Mechanism of Hydrogen Peroxide Formation on Sprayed Water Microdroplets. *J. Am. Chem. Soc.* **2023,** *145* (30), 16315-16317.
(68) Qiu, L.; Cooks, R. G., Spontaneous Oxidation in Aqueous Microdroplets: Water Radical Cation as Primary Oxidizing Agent. *Angew. Chem. Int. Ed.* **2024,** *136* (17), e202400118.
(69) Kathmann, S. M.; Kuo, I. F. W.; Mundy, C. J., Electronic Effects on the Surface Potential at the Vapor−Liquid Interface of Water. *J. Am. Chem. Soc.* **2008,** *130* (49), 16556-16561.
(70) Cendagorta, J. R.; Ichiye, T., The Surface Potential of the Water–Vapor Interface from Classical Simulations. *J. Phys. Chem. B* **2015,** *119* (29), 9114-9122.
(71) Corey, E. J., Catalytic Enantioselective Diels–Alder Reactions: Methods, Mechanistic Fundamentals, Pathways, and Applications. *Angew. Chem. Int. Ed.* **2002,** *41* (10), 1650-1667.
(72) Pindur, U.; Lutz, G.; Otto, C., Acceleration and selectivity enhancement of Diels-Alder reactions by special and catalytic methods. *Chem. Rev.* **1993,** *93* (2), 741-761.
(73) Schlueter, J. A.; Seaman, J. M.; Taha, S.; Cohen, H.; Lykke, K. R.; Wang, H. H.; Williams, J. M., Synthesis, purification, and characterization of the 1 : 1 addition product of C60 and anthracene. *J. Chem. Soc., Chem. Commun.* **1993**, 972-974.
(74) Tsuda, M.; Ishida, T.; Nogami, T.; Kurono, S.; Ohashi, M., Isolation and characterization of Diels–Alder adducts of C60 with anthracene and cyclopentadiene. *J. Chem. Soc., Chem. Commun.* **1993**, 1296-1298.
(75) Banerjee, S.; Gnanamani, E.; Yan, X.; Zare, R. N., Can all bulk-phase reactions be accelerated in microdroplets? *Analyst* **2017,** *142* (9), 1399-1402.
(76) Bain, R. M.; Sathyamoorthi, S.; Zare, R. N., "On-Droplet" Chemistry: The Cycloaddition of Diethyl Azodicarboxylate and Quadricyclane. *Angew. Chem. Int. Ed.* **2017,** *56* (47), 15083-15087.
(77) Chen, H.; Wang, R.; Chiba, T.; Foreman, K.; Bowen, K.; Zhang, X., Designer "Quasi-Benzyne": The Spontaneous Reduction of Ortho-Diiodotetrafluorobenzene on Water Microdroplets. *J. Am. Chem. Soc.* **2024,** *146* (15), 10979-10983.
(78) Aragonès, A. C.; Haworth, N. L.; Darwish, N.; Ciampi, S.; Bloomfield, N. J.; Wallace, G. G.; Diez-Perez, I.; Coote, M. L., Electrostatic catalysis of a Diels–Alder reaction. *Nature* **2016,** *531* (7592), 88-91.
(79) Kühne, T. D.; Iannuzzi, M.; Del Ben, M.; Rybkin, V. V.; Seewald, P.; Stein, F.; Laino, T.; Khaliullin, R. Z.; Schütt, O.; Schiffmann, F.; Golze, D.; Wilhelm, J.; Chulkov, S.; Bani-Hashemian, M. H.; Weber, V.; Borštnik, U.; Taillefumier, M.; Jakobovits, A. S.; Lazzaro, A.; Pabst, H.; Müller, T.; Schade, R.; Guidon, M.; Andermatt, S.; Holmberg, N.; Schenter, G. K.; Hehn, A.; Bussy, A.; Belleflamme, F.; Tabacchi, G.; Glöß, A.; Lass, M.; Bethune, I.; Mundy, C. J.; Plessl, C.; Watkins, M.; VandeVondele, J.; Krack, M.; Hutter, J., CP2K: An electronic structure and molecular dynamics software package - Quickstep: Efficient and accurate electronic structure calculations. *J. Chem. Phys.* **2020,** *152* (19), 194103.
(80) Barducci, A.; Bussi, G.; Parrinello, M., Well-Tempered Metadynamics: A Smoothly Converging and Tunable Free-Energy Method. *Phys. Rev. Lett.* **2008,** *100* (2), 020603.
(81) Goedecker, S.; Teter, M.; Hutter, J., Separable dual-space Gaussian pseudopotentials. *Phys. Rev. B* **1996,** *54* (3), 1703.
(82) Hartwigsen, C.; Gœdecker, S.; Hutter, J., Relativistic separable dual-space Gaussian pseudopotentials from H to Rn. *Phys. Rev. B* **1998,** *58* (7), 3641.
(83) VandeVondele, J.; Hutter, J., Gaussian basis sets for accurate calculations on molecular systems in gas and condensed phases. *J. Chem. Phys.* **2007,** *127* (11), 114105.
(84) Becke, A. D., Density-functional exchange-energy approximation with correct asymptotic behavior. *Phys. Rev. A* **1988,** *38* (6), 3098.
(85) Frisch, M.; Trucks, G.; Schlegel, H.; Scuseria, G.; Robb, M.; Cheeseman, J.; Scalmani, G.; Barone, V.; Petersson, G.; Nakatsuji, H., Gaussian 16, Revision A. 03, Gaussian. *Inc., Wallingford CT* **2016,** *3*.
(86) Krishnan, R.; Binkley, J. S.; Seeger, R.; Pople, J. A., Self-consistent molecular orbital methods. XX. A basis set for correlated wave functions. *J. Chem. Phys.* **1980,** *72* (1), 650-654.
(87) Zhao, Y.; Truhlar, D. G., The M06 suite of density functionals for main group thermochemistry, thermochemical kinetics, noncovalent interactions, excited states, and transition elements: two new functionals and systematic testing of four M06-class functionals and 12 other functionals. *Theor. Chem. Acc.* **2008,** *120* (1), 215-241.
(88) Thomas, L. L.; Tirado-Rives, J.; Jorgensen, W. L., Quantum Mechanical/Molecular Mechanical Modeling Finds Diels−Alder Reactions Are Accelerated Less on the Surface of Water Than in Water. *J. Am. Chem. Soc.* **2010,** *132* (9), 3097-3104.
(89) Di Pino, S.; Perez Sirkin, Y. A.; Morzan, U. N.; Sánchez, V. M.; Hassanali, A.; Scherlis, D. A., Water Self-Dissociation is Insensitive to Nanoscale Environments. *Angew. Chem. Int. Ed.* **2023,** *62* (34), e202306526.
(90) Pestana, L. R.; Hao, H.; Head-Gordon, T., Diels–Alder Reactions in Water Are Determined by Microsolvation. *Nano Lett.* **2020,** *20* (1), 606-611.
(91) Chandrasekhar, J.; Shariffskul, S.; Jorgensen, W. L., QM/MM Simulations for Diels−Alder Reactions in Water: Contribution of Enhanced Hydrogen Bonding at the Transition State to the Solvent Effect. *J. Phys. Chem. B* **2002,** *106* (33), 8078-8085.
(92) Soto-Delgado, J.; Tapia, R. A.; Torras, J., Multiscale Treatment for the Molecular Mechanism of a Diels–Alder Reaction in Solution: A QM/MM-MD Study. *J. Chem. Theory Comput.* **2016,** *12* (10), 4735-4742.
(93) Cassone, G., Nuclear Quantum Effects Largely Influence Molecular Dissociation and Proton Transfer in Liquid Water under an Electric Field. *J. Phys. Chem. Lett.* **2020,** *11* (21), 8983-8988.

(94) Cassone, G.; Pietrucci, F.; Saija, F.; Guyot, F.; Saitta, A. M., One-step electric-field driven methane and formaldehyde synthesis from liquid methanol. *Chem. Sci.* **2017,** *8* (3), 2329-2336.
(95) Cassone, G.; Sofia, A.; Rinaldi, G.; Sponer, J., Catalyst-Free Hydrogen Synthesis from Liquid Ethanol: An ab Initio Molecular Dynamics Study. *J. Phys. Chem. C* **2019,** *123* (14), 9202-9208.
(96) Fried, S. D.; Bagchi, S.; Boxer, S. G., Extreme electric fields power catalysis in the active site of ketosteroid isomerase. *Science* **2014,** *346* (6216), 1510-1514.
(97) Shaik, S.; Ramanan, R.; Danovich, D.; Mandal, D., Structure and reactivity/selectivity control by oriented-external electric fields. *Chem. Soc. Rev.* **2018,** *47* (14), 5125-5145.
(98) Welborn, V. V.; Ruiz Pestana, L.; Head-Gordon, T., Computational optimization of electric fields for better catalysis design. *Nat. Catal.* **2018,** *1* (9), 649-655.
(99) Zhang, Y.; Jiang, B., Universal machine learning for the response of atomistic systems to external fields. *Nat. Commun.* **2023,** *14* (1), 6424.
(100) Shaik, S. S.; Stuyver, T., *Effects of electric fields on structure and reactivity: new horizons in chemistry*. Royal Society of Chemistry: 2021.
(101) Meir, R.; Chen, H.; Lai, W.; Shaik, S., Oriented electric fields accelerate Diels–Alder reactions and control the endo/exo selectivity. *ChemPhysChem* **2010,** *11* (1), 301-310.
(102) Ramanan, R.; Danovich, D.; Mandal, D.; Shaik, S., Catalysis of Methyl Transfer Reactions by Oriented External Electric Fields: Are Gold–Thiolate Linkers Innocent? *J. Am. Chem. Soc.* **2018,** *140* (12), 4354-4362.
(103) Hoffmann, N. M.; Wang, X.; Berkelbach, T. C., Linear Free Energy Relationships in Electrostatic Catalysis. *ACS Catal.* **2022,** *12* (14), 8237-8241.
(104) Yu, S.; Vermeeren, P.; Hamlin, T. A.; Bickelhaupt, F. M., How Oriented External Electric Fields Modulate Reactivity. *Chem. Eur. J.* **2021,** *27* (18), 5683-5693.
(105) Martins-Costa, M. T. C.; Ruiz-López, M. F., Electrostatics and Chemical Reactivity at the Air–Water Interface. *J. Am. Chem. Soc.* **2023,** *145* (2), 1400-1406.
(106) Lin, S.; Cao, L. N. Y.; Tang, Z.; Wang, Z. L., Size-dependent charge transfer between water microdroplets. *Proc. Natl. Acad. Sci.* **2023,** *120* (31), e2307977120.
(107) Müller, T.; Badu-Tawiah, A.; Cooks, R. G., Accelerated Carbon-Carbon Bond-Forming Reactions in Preparative Electrospray. *Angew. Chem. Int. Ed.* **2012,** *51* (47), 11832-11835.
(108) Bain, R. M.; Pulliam, C. J.; Thery, F.; Cooks, R. G., Accelerated Chemical Reactions and Organic Synthesis in Leidenfrost Droplets. *Angew. Chem. Int. Ed.* **2016,** *55* (35), 10478-10482.
(109) Bain, R. M.; Pulliam, C. J.; Cooks, R. G., Accelerated Hantzsch electrospray synthesis with temporal control of reaction intermediates. *Chem. Sci.* **2015,** *6* (1), 397-401.
(110) Yan, X.; Bain, R. M.; Cooks, R. G., Organic Reactions in Microdroplets: Reaction Acceleration Revealed by Mass Spectrometry. *Angew. Chem. Int. Ed.* **2016,** *55* (42), 12960-12972.
(111) Parlar, H.; Baumann, R., Diels-Alder Reaction of Cyclopentadiene with Acrylic Acid Derivatives in Heterogeneous Phases. *Angew. Chem. Int. Ed.* **1981,** *20* (12), 1014-1014.
(112) Dickson, R. S.; Dobney, B. J.; Eastwood, F. W., Preparation of cyclopentadiene from its dimer. *J. Chem. Educ.* **1987,** *64* (10), 898.
(113) Rideout, D. C.; Breslow, R., Hydrophobic acceleration of Diels-Alder reactions. *J. Am. Chem. Soc.* **1980,** *102* (26), 7816-7817.
(114) Haddad, R.; Sparrapan, R.; Eberlin, M. N., Desorption sonic spray ionization for (high) voltage-free ambient mass spectrometry. *Rapid Commun. Mass Spectrom.* **2006,** *20* (19), 2901-2905.
(115) Hirabayashi, A.; Sakairi, M.; Koizumi, H., Sonic Spray Ionization Method for Atmospheric Pressure Ionization Mass Spectrometry. *Anal. Chem.* **1994,** *66* (24), 4557-4559.
(116) Banerjee, S.; Mazumdar, S., Electrospray Ionization Mass Spectrometry: A Technique to Access the Information beyond the Molecular Weight of the Analyte. *Int. J. Anal. Chem.* **2012,** *2012* (1), 282574.
(117) Gao, D.; Jin, F.; Lee, J. K.; Zare, R. N., Aqueous microdroplets containing only ketones or aldehydes undergo Dakin and Baeyer–Villiger reactions. *Chem. Sci.* **2019,** *10* (48), 10974-10978.